Coupling-Dependent Data Flipping in Wireless Power and Data Transfer System

Hao Qiu, Takayasu Sakurai, and Makoto Takamiya
Institute of Industrial Science
The University of Tokyo, Tokyo, Japan
Email: hqiu@iis.u-tokyo.ac.jp

***Abstract*—Load modulation is a common method to transfer data from the receiver (RX) side to the transmitter (TX) side in a magnetic resonance coupling wireless power transfer system. However, coupling-dependent data flipping (CDDF), that the data can be flipped depending on the coupling between TX and RX coils, is found for the first time using the conventional voltage monitoring across the TX coil. An analytic formula of the critical coupling coefficient (k_C) of the coils that determines CDDF is derived. To avoid CDDF, a TX input voltage monitoring method is proposed. Both the CDDF in the conventional method and the correct data transfer without CDDF in the proposed method are demonstrated in the measurement.**

Keywords—Coupling-dependent data flipping, critical coupling coefficient, load modulation, magnetic resonance coupling, transmitter input voltage monitoring, wireless power transfer, wireless data transfer

I. Introduction

Wireless power transfer using magnetic resonance coupling has been applied in a wide range of subjects such as electric vehicles, mobile devices, and biomedical implants [1]. In a wireless power transfer system, when the coupling coefficient (k) between the TX and RX coils changes, both the coil-to-coil efficiency [2] and power losses in circuit components [3-4] are affected. In order to control and regulate the power in the RX coil, the establishment of a RX-to-TX communication (uplink) which is irrespective of k is required. As is shown in Fig. 1, in a wireless power and data transfer system, load modulation [5] has been widely used due to its simple architecture in which the change of the RX coil's loading condition is reflected in the TX coil and the voltage across the TX coil (V_L) is monitored. However, most of the previous research [6-8] has focused on the case where k is a constant and few has discussed its possible effects.

II. CDDF and the Solution

In this work, the effects of k on data transfer in a wireless power and data transfer system are discussed. As shown in Fig. 2(a), when k is smaller than a critical k (k_C), the data are demodulated depending on the amplitude of V_L. Here, data '1' is defined as large V_L and data '0' is defined as small V_L. When $k > k_C$, on the other hand, the relation between the data and the amplitude of V_L is flipped and incorrect data are demodulated, which we call coupling-dependent data flipping (CDDF). k_C is the critical point, at which V_L does not change its value during load modulation and thus data cannot be transferred from the RX side to the TX side. Thus, we propose to monitor the TX input voltage (V_{LC}) rather than V_L in Fig. 1. As shown in Fig. 2(b), where data '1' is defined as small V_{LC} and data '0' is defined as large V_{LC}, an uplink with a correct data transfer robust against CDDF is established.

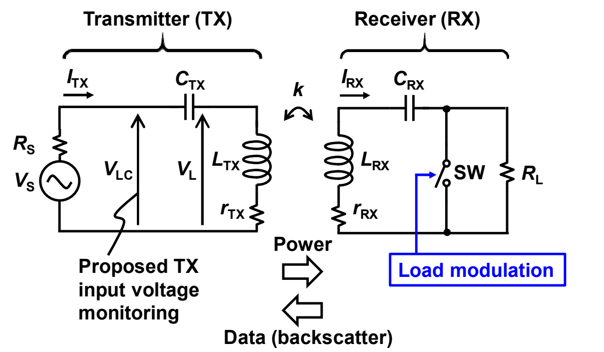

Fig. 1. Equivalent circuit model of a wireless power and data transfer system. The impedance matching networks (IMNs) in both TX and RX sides are not drawn for simplicity.

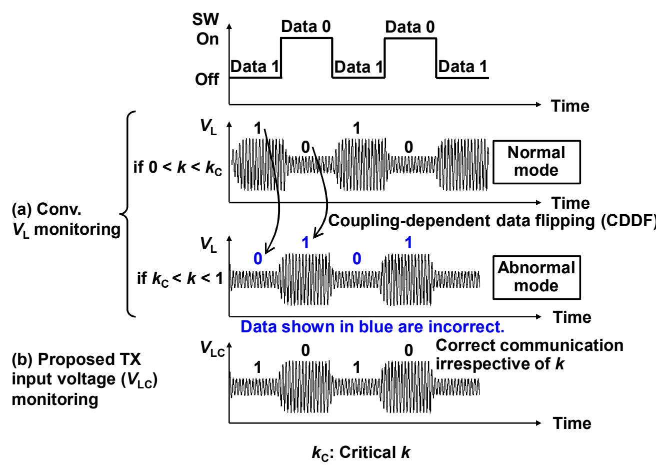

Fig. 2. Data backscatter based on (a) conventional V_L monitoring and (b) proposed V_{LC} monitoring.

III. Circuit Analysis of CDDF

In this chapter, the origin of CDDF is analyzed. Fig. 1 shows the equivalent circuit model of a series-series topology,

978-1-7281-0397-6/19/$31.00 ©2019 IEEE

where the inductors and compensation capacitors are connected in series in both TX and RX sides. The TX side, consisting of an inductor (L_{TX}) with an equivalent series resistance (r_{TX}) and a compensation capacitor (C_{TX}), is driven by a voltage source (V_S) with an internal resistance (R_S). The RX side is composed of an inductor (L_{RX}) with an equivalent series resistance (r_{RX}) and a compensation capacitor (C_{RX}). R_L is the load resistance. The currents flowing in the TX and RX sides are I_{TX} and I_{RX}, respectively.

Applying Kirchhoff's voltage law to the circuit, we obtain the following relations between the currents and voltages at the resonance frequency (f_0):

$$\begin{cases} \omega_0 = 2\pi f_0 = 1/\sqrt{L_{TX}C_{TX}} = 1/\sqrt{L_{RX}C_{RX}} \\ V_S = I_{TX}(R_S + r_{TX} + j\omega_0 L_{TX} + 1/(j\omega_0 C_{TX})) - j\omega_0 M I_{RX} \\ j\omega_0 M I_{TX} = I_{RX}(R_L + r_{RX} + j\omega_0 L_{RX} + 1/(j\omega_0 C_{RX})) \\ M = k\sqrt{L_{TX}L_{RX}} \end{cases} . \quad (1)$$

Here, M is the mutual inductance between the TX and RX coils. j is the imaginary unit.

The ratio of V_L to V_S at f_0 can be described as:

$$\begin{aligned} \frac{V_L}{V_S} &= \frac{I_{TX}(j\omega_0 L_{TX} + r_{TX}) - I_{RX} j\omega_0 M}{V_S} \\ &= \frac{(R_L + r_{RX})(j\omega_0 L_{TX} + r_{TX}) + \omega_0^2 k^2 L_{TX} L_{RX}}{(R_S + r_{TX})(R_L + r_{RX}) + \omega_0^2 k^2 L_{TX} L_{RX}} . \end{aligned} \quad (2)$$

Its amplitude is:

$$\left|\frac{V_L}{V_S}\right| = \frac{\sqrt{(R_L + r_{RX})^2 \omega_0^2 L_{TX}^2 + \left[(R_L + r_{RX}) r_{TX} + \omega_0^2 k^2 L_{TX} L_{RX}\right]^2}}{(R_S + r_{TX})(R_L + r_{RX}) + \omega_0^2 k^2 L_{TX} L_{RX}} . \quad (3)$$

Based on the design parameters listed in Table I, a numerical calculation was performed. Fig. 3 shows k dependence of the calculated $|V_L/V_S|$ in the conventional V_L monitoring. k_C is defined when

$$\left|V_L / V_S\right|_{R_L} = \left|V_L / V_S\right|_{R_L = 0\Omega} . \quad (4)$$

It can be clearly seen that the data flips in the abnormal mode when $k > k_C$ (~0.26). To understand the key parameters determining k_C, we derived its analytic formula by assuming r_{TX} and r_{RX} as zero. That is:

$$k_C = \sqrt{\frac{R_L(\omega_0^2 L_{TX}^2 - R_S^2)}{2R_S \omega_0^2 L_{TX} L_{RX}}} . \quad (5)$$

Since ω_0, L_{TX}, L_{RX} are determined by the coil design, we discuss the dependence of k_C on R_L and R_S. The R_L dependence of k_C is shown in Fig. 4(a), where R_S equals 50Ω. Equation (5) gives the same positive R_L dependence as the numerical calculation based on (4), though with a deviation which comes from neglecting r_{TX} and r_{RX}. This deviation becomes smaller when R_L becomes larger. The R_S dependence of k_C is shown in Fig. 4(b), where R_L equals 10Ω. When R_S becomes smaller than 5Ω, k_C will become larger than 1 and CDDF cannot occur.

TABLE I. PARAMETERS OF TX AND RX COILS

	TX coil	RX coil
Coil diameter	300 mm	
Coil thickness	19 mm	14 mm
Wire diameter	1 mm	
Coil turns	10	
Resonance frequency (f_0)	153 kHz	
Inductor	L_{TX}=66.2 μH	L_{RX}=73.8 μH
Equivalent series resistance (ESR)	r_{TX}=0.5 Ω	r_{RX}=1.0 Ω
Compensation capacitor	C_{TX}=16.4 nF	C_{RX}=14.7 nF
Quality factor	127	71

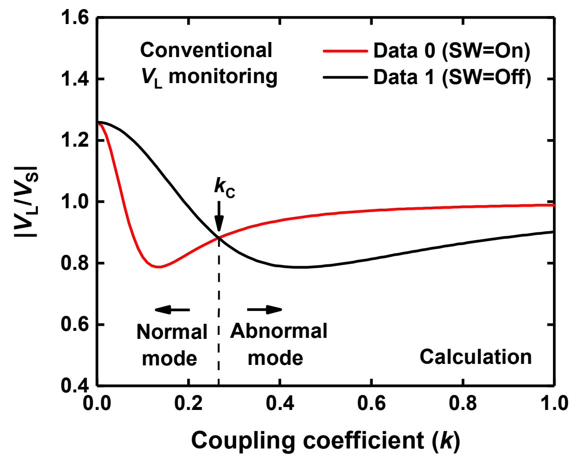

Fig. 3. k dependence of calculated $|V_L/V_S|$.

However, the impedance matching networks (IMNs) are usually inserted in both TX and RX sides to optimize the power transfer efficiency, and thus R_S seen from the TX coil's point of view equals R_L [9]. Thus, in the conventional V_L monitoring, CDDF cannot be avoided.

On the other hand, in the proposed V_{LC} monitoring, the amplitude of the ratio of V_{LC} to V_S at f_0 is described as:

$$\begin{aligned} \left|\frac{V_{LC}}{V_S}\right| &= 1 - \frac{I_{TX} r_{TX}}{V_S} \\ &= 1 - \frac{(R_L + r_{RX}) R_S}{(R_S + r_{TX})(R_L + r_{RX}) + \omega_0^2 k^2 L_{TX} L_{RX}} . \end{aligned} \quad (6)$$

Fig. 5 shows k dependence of the calculated $|V_{LC}/V_S|$ in the proposed V_{LC} monitoring. It is seen that, irrespective of k,

$$\left|V_{LC} / V_S\right|_{R_L} < \left|V_{LC} / V_S\right|_{R_L = 0\Omega} . \quad (7)$$

That means CDDF never happens with V_{LC} monitoring and an uplink with a correct data transfer can be established.

Before discussing the measurement results, we give more explanations of why k_C exists in the conventional V_L monitoring and why CDDF never happens in the proposed V_{LC} monitoring. Fig. 6 gives the simplified circuit model of Fig. 1, assuming r_{TX} and r_{RX} to be zero. The equivalent resistance (r)

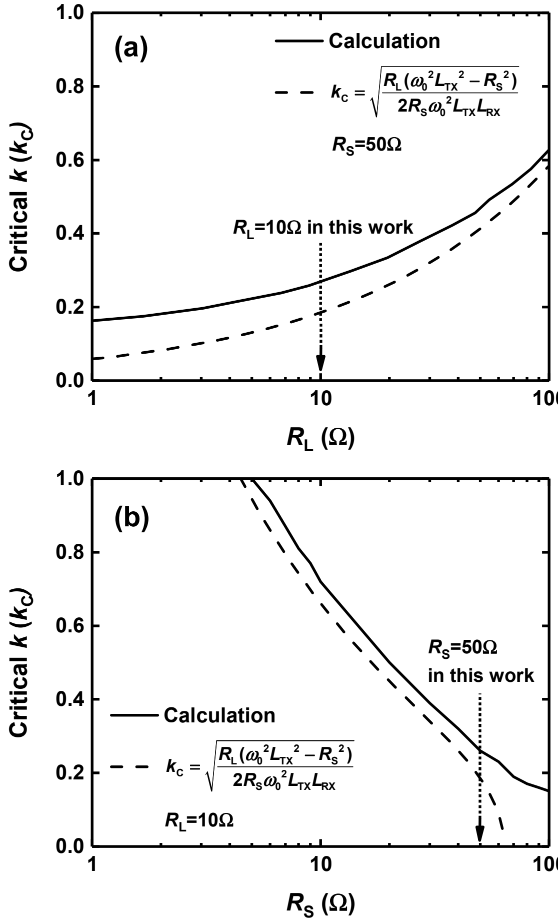

Fig. 4. (a) R_L and (b) R_S dependence of calculated k_C.

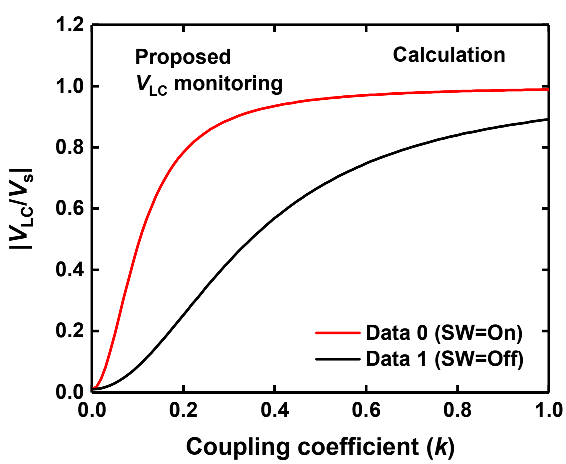

Fig. 5. k dependence of calculated $|V_{LC}/V_S|$.

of the RX side seen from the TX side at f_0 can be described as [10]:

$$r = \omega_0^2 k^2 L_{TX} L_{RX} / R_L. \tag{8}$$

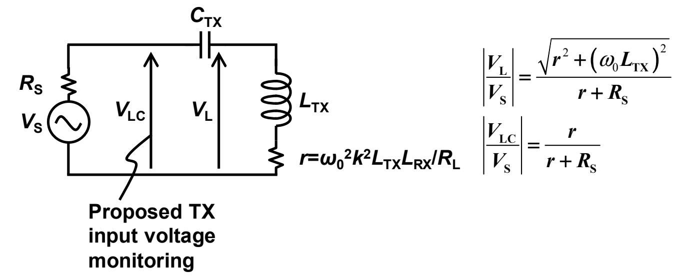

Fig. 6. Simplified circuit model of Fig. 1, in which r_{TX} and r_{RX} are assumed to be zero. r is the equivalent resistance of the RX side seen from the TX side.

$|V_L/V_S|$ at f_0 is

$$\left|\frac{V_L}{V_S}\right| = \frac{\sqrt{r^2+(\omega_0 L_{TX})^2}}{r+R_S}. \tag{9}$$

$|V_L/V_S|$ equals 1 when R_L is shorted. When R_L is loaded, since r depends on k, k_C can exist to satisfy that

$$\sqrt{r^2+\omega_0^2 L_{TX}^2} = r + R_S. \tag{10}$$

At that point, $|V_L/V_S|$ also equals 1, which makes (4) hold.

On the other hand, $|V_{LC}/V_S|$ at f_0 is

$$\left|\frac{V_{LC}}{V_S}\right| = \frac{r}{r+R_S}. \tag{11}$$

It can be easily seen that (7) holds based on (8) and (11).

IV. Experimental Results

Fig. 7 shows the photo of the fabricated coils based on the parameters in Table I. A signal generator with R_S=50Ω was used to generate a sinusoidal wave signal at 153kHz. k was measured according to the method described in [11] and efficiency (η) is defined as the ratio of the power directly transferred to R_L to the power extracted from the power source [10]. Fig. 8 gives the dependence of measured k and η on the distance (d) between the TX and RX coils.

Fig. 9 shows k dependence of measured $|V_L/V_S|$. k_C exists, as predicted in Fig.3. Compared with the calculation results, measured $|V_L/V_S|$ matches well when SW is Off but shows a deviation when SW is On. It can be ascribed to the unavoidable fact that the f_0 of the TX and RX coils can mismatch and the reflected reactance from the RX side will then affect the TX side. The effect is greater when SW is On. This is also the reason why the measured k_C (~0.43) in Fig. 9 does not match the calculated k_C (~0.26) in Fig. 3.

On the other hand, Fig. 10 shows the k dependence of measured $|V_{LC}/V_S|$ we proposed. As predicted in Fig. 5, (7) holds irrespective of k and CDDF never happens in the proposed V_{LC} monitoring. In addition, measured $|V_{LC}/V_S|$ in Fig. 10 matches calculation results in Fig. 5 well, which is different from the results of $|V_L/V_S|$ especially when SW is On. This is

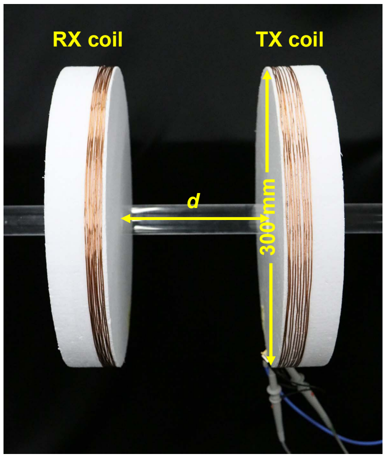

Fig. 7. Photo of TX and RX coils.

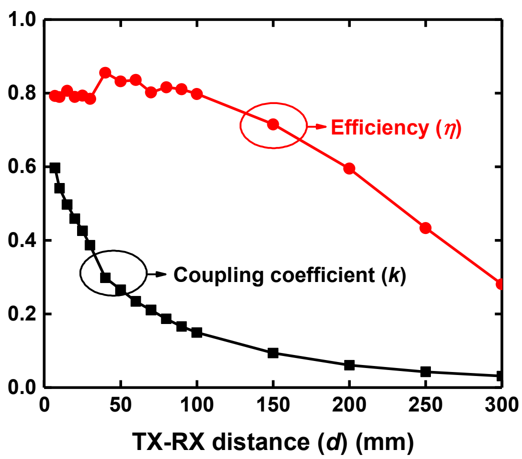

Fig. 8. d dependence of measured k and η.

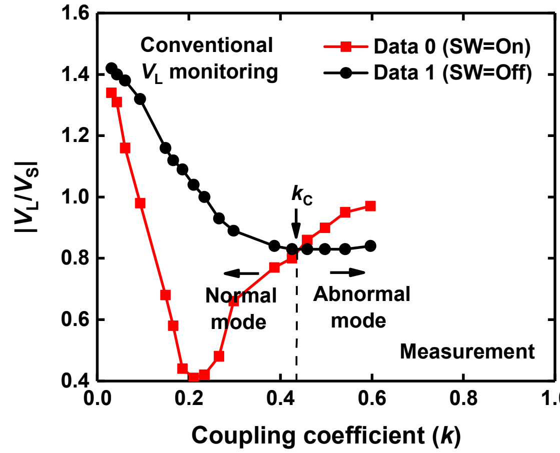

Fig. 9. k dependence of measured $|V_L/V_S|$.

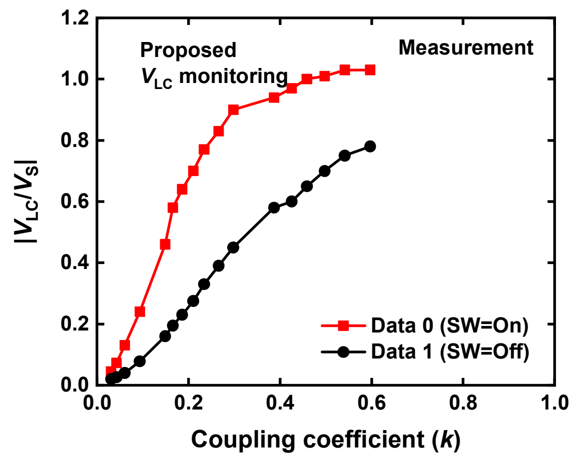

Fig. 10. k dependence of measured $|V_{LC}/V_S|$.

another advantage of the proposed V_{LC} monitoring that it supports an uplink robust against f_0 variations compared with the conventional V_L monitoring.

Here, more discussions are given. Series-series topology has been analyzed in this work, analyses in series-parallel, parallel-series, and parallel-parallel topologies will be included in our future work. In addition, the coil parameters were chosen mainly for EV applications. The universality of the phenomenon of CDDF will be discussed in several other application scenarios, such as mobile charging and biomedical applications.

V. Conclusions

To the best of our knowledge, the issue of CDDF was found for the first time in a wireless power and data transfer system. An analytic formula of k_C which shows a CDDF boundary was also derived. In order to solve CDDF, we proposed to monitor the transmitter input voltage (V_{LC}). Circuit analysis and measurement were performed to demonstrate our conclusions.

Acknowledgment

This work was partially supported by JST ERATO Grant Number JPMJER1501, Japan.

References

[1] M. Kiani and M. Ghovanloo, "The circuit theory behind coupled-mode magnetic resonance-based wireless power transmission," *IEEE Trans. Circuits Syst. I, Reg. Papers*, vol. 59, no. 9, pp. 2065–2074, Sep. 2012.

[2] H. Qiu, Y. Narusue, Y. Kawahara, T. Sakurai, and M. Takamiya, "Digital coil: transmitter coil with programmable radius for wireless powering against distance variation," in *IEEE Wireless Power Transfer Conf.*, Jun. 2018, pp. 1–4.

[3] A. Ayachit, F. Corti, A. Reatti, and M. Kazimierczuk, "Zero-voltage switching operation of transformer class-E inverter at any coupling coefficient," *IEEE Trans. Ind. Electron.*, vol. 66, no. 3, pp. 1809–1819, Mar. 2019.

[4] T. Nagashima, X. Wei, E. Bou, E. Alarcon, M. K. Kazimierczuk, and H. Sekiya, "Analysis and design of loosely inductive coupled wireless power transfer system based on class-E2 DC-DC converter for efficiency enhancement," *IEEE Trans. Circuits Syst. I, Reg. Papers*, vol. 62, no. 11, pp. 2781–2791, Nov. 2015.

[5] X. Shi, A. N. Parks, B. H. Waters, and J. R. Smith, "Co-optimization of efficiency and load modulation data rate in a wireless power transfer system," in *Proc. IEEE Int. Symp. Circuits Syst.*, May 2015, pp. 698–701.

[6] Y. Jang, J. Han, S. Cho, G. Moon, J. Kim, and H. Sohn, "Wireless power and data transfer system for smart bridge sensors," in *Proc. IEEE Appl. Power Electron. Conf. Expo.*, Mar. 2016, pp. 3690–3696.

[7] I. Nam, R. Dougal, and E. Santi, "Novel control approach to achieving efficient wireless battery charging for portable electronic devices," in *Proc. IEEE Energy Convers. Congr. Expo.*, Sept. 2012, pp. 2482–2491.

[8] H.-M. Lee, H. Park, and M. Ghovanloo, "A power-efficient wireless system with adapative supply control for deep brain stimulation," *IEEE J. Solid-State Circuits*, vol. 48, no. 9, pp. 2203–2216, Sep. 2013.

[9] E. Bou, R. Sedwick, and E. Alarcon, "Maximizing efficiency through impedance matching from a circuit-centric model of non-radiative resonant wireless power transfer," in *Proc. IEEE Int. Symp. Circuits Syst.*, May 2013, pp. 29–32.

[10] M. Fu, H. Yin, X. Zhu, and C. Ma, "Analysis and tracking of optimal load in wireless power transfer systems," *IEEE Trans. Power Electron.*, vol. 30, no. 7, pp. 3952–3963, Jul. 2015.

[11] K. Hata, T. Imura, and Y. Hori, "Simplified measuring method of kQ product for wireless power transfer via magnetic resonance coupling based on input impedance measurement," in *Proc. IEEE IECON*, Oct. 2017, pp. 6974–6979.